A EUROPEAN JOURNAL

CHEMPHYSCHEM

OF CHEMICAL PHYSICS AND PHYSICAL CHEMISTRY

Accepted Article

Title: Flow pattern characterization of Biphasic Electrochemical Cells by MRI under forced hydrodynamic conditions

Authors: Maria Raquel Serial, Manuel Isaac Velasco, Emilia V. Silletta, Franco M. Zanotto, Sergio A. Dassie, and Rodolfo H. Acosta

To be cited as: *ChemPhysChem* 10.1002/cphc.201700775

Link to VoR: http://dx.doi.org/10.1002/cphc.201700775

A Journal of

ChemPubSoc Europe

WILEY-VCH

www.chemphyschem.org

ARTICLE WILEY-VCH

Flow pattern characterization of Biphasic Electrochemical Cells by MRI under forced hydrodynamic conditions.

María R. Serial,[a] Manuel I. Velasco,[a] Emilia V. Silletta,[a] Franco M. Zanotto,[b] Sergio A. Dassie,[b] and Rodolfo H. Acosta*[a]

Abstract: Fluid dynamics of a liquid|liquid system inside a four-electrode electrochemical cell is studied by velocimetry MRI and flow propagators measurements. In order to fully characterize this system, three different cell configurations were analyzed, operating at two rotational frequencies. Quantitative information about the stability of the liquid|liquid interface and the dynamics of the organic phase are determined. NMR results are in agreement with electrochemical measurements carried out using the same experimental setup.

Introduction

The use of electrochemical cells to study biphasic systems where two immiscible electrolyte solutions develop an interface (ITIES) have been widely used to study processes such as ion transfer across liquid|liquid interfaces [1] under forced hydrodynamic conditions. [2] These kind of charge transfer processes are relevant in a wide variety of fields such as phase transfer catalysis or electro-catalysis, analytical determinations and extractions; in addition to the biomimetic features that the biphasic system provides.[1] Many of these applications imply the use of an experimental setup similar to that of a rotating disk electrode (RDE). In these devices, two immiscible electrolyte solutions are placed in different compartments of a cell, which are connected by a small hole, and convection is induced in one of the compartments by a cylindrical rotating rod. It is then clear that the measured electrochemical signals will depend on the system hydrodynamics. Moreover, the correct modeling of the electrochemical response yields a good understanding of the flow patterns.

RDE cells have been extensively studied theoretically, by means of computational fluid dynamics (CFD) [3] and by magnetic resonance imaging (MRI).[4] However, the hydrodynamic of the biphasic RDE cell has not been yet extensively studied. A common approach that helps in the simplification of the mathematical framework that describes electrochemical responses is to maintain one of the fluids still while flow is induced in another. Recently we presented a new description for the determination of the partition coefficient of neutral weak bases using a liquid|liquid interface with forced hydrodynamic conditions, where CFD and MRI were used to determine the flow patterns, in particular, the fluid dynamics near the liquid interface.[5] Moreover, for many experimental setups, luggin capillaries are used. For instance, in order to perform quantitative measurements of current or potential at the interface between two immiscible electrolyte solutions, only a four-electrode setup with capillaries near the interface can provide reliable electrochemical measurements of ion transfer at ITIES. It is expected that their presence will have an impact on the flow dynamics that has not been addressed so far.

Determination of flow velocity by MRI has been used in different applications in fields such as industry, chemistry, and clinics.[6] Even though the time resolution is below that achieved by particle imaging velocimetry (PIV)[7] or laser Doppler anemometry (LDA),[8] MRI has the advantage that no tracer particles are required, and that non-transparent fluid or opaque containers can be used. The most characterized system that shares similar aspects with the velocity pattern found in an electrochemical cell (ECC) is the one involving a Couette Cell (CC). This device is composed of two concentric cylinders, where a large variety of flows can occur upon variations of the fluid properties, cell geometry, or rotation rates. [9] Several studies have been focused on the characterization of the velocity pattern inside this device in order to collect rheological information of complex fluids, such as wormlike micelles[10] and ionic liquid colloidal suspensions.[11] In addition, special attention has been paid to the study of secondary flow formation in a CC. When the rotating inner cylinder exceeds a critical value, a particular instability characterized by the presence of counter-rotating vortex pairs (Taylor Vortex Flow, TVF) is formed in the fluid. Several works have successfully used MRI to visualize the velocity in TVF,[12] probing rapidly changing systems such as translating Taylor vortices found in vortex flow reactors and also characterizing TVF in axially stratified two fluid systems.[13]

In this work, we perform a full characterization of the flow patterns in both, a model and an operating biphasic ITIES cells for different rotating frequencies. In addition to the acquired velocity maps, the velocity propagator,[14] namely the probability of a particle moving from one point in space to another in a given period of time, is obtained for different regions in the cell in order to provide information on the symmetry of the flow patterns. We find that the velocity pattern of the liquid surrounding the rotating rod is very similar to those found in CC, while a rotational vortex is present below the rotating rod. In addition, fluid dynamics in the interfacial area is also explored. Finally, simple ion transfer (tetraethylammonium transfer) and facilitated ion transfer (potassium ion transfer assisted by DB18C6) across a water|1,2-dichloroethane interface have been used as

[a] Lic. M.R. Serial, Dr. M.I. Velasco, Dr. E.V. Silleta, Dr. R.H. Acosta
FAMAF-Universidad Nacional de Córdoba and IFEG-CONICET
5000, Ciudad Universitaria, Córdoba, Argentina
E-mail: racosta@famaf.unc.edu.ar
[b] Lic. F.M. Zanotto, Dr. S.A. Dassie
Instituto de Investigaciones en Fisicoquímica de córdoba (INFIQC) – CONICET, Departamento de Fisicoquímica, Facultad de Ciencias Químicas, Universidad Nacional de Córdoba
5000, Ciudad Universitaria, Córdoba, Argentina

Supporting information for this article is given via a link at the end of the document

descriptors for the stability of the interface and the movement of the fluid in the phase under quiescent conditions.

Electrochemical cells

Electrochemical measurements at the liquid|liquid interface between two immiscible fluids are generally performed using a non-conventional ECC combined with a four-electrode setup.[1b, 15] In order to describe the hydrodynamics inside this system, three different configurations of electrochemical cells were studied, as schematized in Fig. 1. Initially, the hydrodynamics of water are described in a single compartment cell, with the exterior container and rotating rod built in acrylic. As all the components of this cell are perfectly aligned and symmetrical with respect to the rotation axis, Z, it is used as a reference. For a model biphasic cell, a glass container is used, as the organic solvent employed (1,2-dichloroethane) swells and dissolves the poly(methyl methacrylate). The inherent misalignments due to the glassware construction impact on the flow patterns. In this setup, the interface between both fluids is established at a small hole in the glass that separates them (Fig. 1b). Finally, the four-electrode cell is studied. In this configuration, two reference electrodes, one for each phase, are needed to monitor the polarization of the liquid|liquid interface during electrochemical experiments. This is accomplished by two luggin capillaries placed in the upper and lower chamber of the cell (Fig. 1c). For the NMR experiments, the ECC was modified in order to fit inside a 25 mm radiofrequency coil (See Experimental Section). For both biphasic cells the lower compartment is filled with 1,2-dichloroethane, generally used as a solvent in the organic phase [1b, 1c] and the upper compartment is filled with water, serving as an aqueous phase. Agitation of only the aqueous phase with the rotating rod was carried out in all the experiments.

Velocities determined by NMR

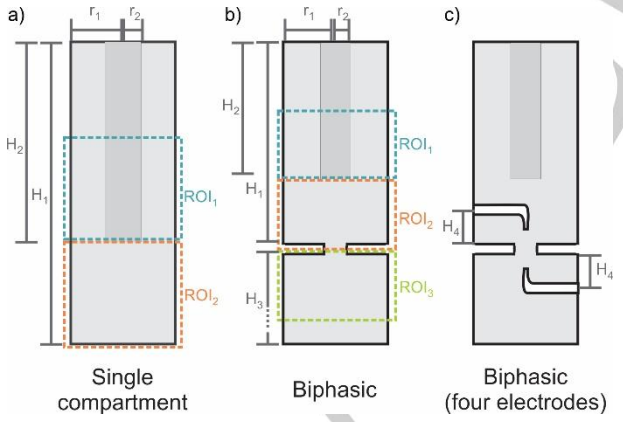

Figure 1: Schematic representation of the different cell configurations studied in this work: (a) single compartment ECC, (b) biphasic ECC and (c) biphasic with four electrodes ECC. In all cases, the axial dimension of the cells exceeded the NMR sensitive volume. Regions of Interest (ROI) are indicated for each configuration. Cell's dimensions are presented in Table S1 of the Supporting Information.

There are two main approaches for the determination of velocities by NMR. One strategy is to acquire a set of images of the desired fluid in motion conditions with and without the application of motion-sensitive gradients. Thus the determination of velocities in a pixel by pixel basis can be achieved. The second approach is to encode the displacement probability in a given direction.[16] A brief description of both methods is given in this section.

MRI is basically a spectroscopic technique, where a spatial dependent frequency is generated by the application of a magnetic field gradient ($\boldsymbol{G}$) which is generally over imposed to the main magnetic field $\boldsymbol{B_0}$ in a pulsed fashion. The frequency that the excited nuclei undergo may be expressed as:

$$\omega(\boldsymbol{r}) = \gamma B_0 + \gamma \boldsymbol{G} \cdot \boldsymbol{r} \quad (1)$$

where γ is the nuclei gyromagnetic ratio and $\boldsymbol{r}$ the nucleus position. The local magnetic field gradient vector $\boldsymbol{G}$ is generated by three independent coils that induce magnetic fields with variations in space that are orthogonal to each other. The acquired signal may be expressed, in a reference frame rotating at the Larmor frequency $\omega_0 = \gamma B_0$, as:

$$s(\boldsymbol{k}) = \int \rho(\boldsymbol{r}) e^{2\pi i \boldsymbol{k}\cdot\boldsymbol{r}}\, d\boldsymbol{k}, \quad (2)$$

where $\boldsymbol{k}$ is the reciprocal-space vector given by $\boldsymbol{k} = \gamma \boldsymbol{G} t/2\pi$, with t being the time the gradient is on. It is clear that a fast Fourier transform (FFT) of the data will render a representation of the object, $\rho(\boldsymbol{r})$. A 3D reconstruction is obtained, either by performing 3D experiments in which each dimension is recorded along an orthogonal direction, or by selecting a number of 2D slices that give a fair representation of the object. In this work, we will focus in a representative 2D image of the central slice of the RDE cells. The MRI pulse sequence employed is schematized in Fig. S1.

When the spin bearing particles are in motion, an extra dephasing is produced due to the displacement in the presence of the magnetic field gradients.[17] In the case of steady-state flow, the phase accumulation due to displacements during the imaging gradients may be ignored, as it is the same for independent image acquisitions. Determination of velocity maps relies on the acquisition of two images for the determination of one velocity component, and four images for the full velocity vector determination in each image pixel. The experiment consists of the acquisition of a reference image and a velocity encoded one, where a pair of bipolar gradient pulses with intensity G_{vel}, duration δ and separation Δ, is introduced. The arbitrary direction of this magnetic field gradient will encode the corresponding velocity component. Subtraction of the phases from the velocity encoded images with the reference image's phase in a pixel by pixel basis will render the distribution of velocity components, assuming a constant velocity within each pixel during the encoding period, as [17]:

$$v_i = \varphi/(\gamma \delta \Delta G_{vel}), \quad (3)$$

where φ is the phase shift for the spin traveling molecule.

The second approach used in this work is the determination of an average propagator $P(\Delta, \boldsymbol{R})$, which is the probability density for molecular displacements $\boldsymbol{R}$ in a time Δ. The pulse sequence shown in Fig. S2 is a pulsed gradient spin echo (PGSE) where displacement encoding gradients amplitude is varied in each acquisition of a 2D experiment. The amplitude of the signal at the echo centre for a fixed displacement time Δ is expressed as [14]:

$$S(\Delta, \boldsymbol{q}) = \int P(\Delta, \boldsymbol{R})\, e^{2\pi i \boldsymbol{R}\cdot\boldsymbol{q}} d\boldsymbol{R} \quad (4)$$

where the wave vector $\boldsymbol{q} = \gamma \boldsymbol{G} \delta / 2\pi$ encodes the displacement in the three orthogonal directions. As the gradients in each direction are applied independently, three individual 2D experiments must be carried out to obtain the full probabilistic information. A FFT on the data on each gradient direction will render the corresponding propagator. In this work, the axes of the average propagator were scaled to the observation time Δ in order to report mean particles velocities.

Results and Discussion

Single compartment cell model. Hydrodynamics in the ECC were studied for two different rotation speeds, 31.4 Hz and 62.8 Hz. Figure 2 shows the velocity maps acquired in all orthogonal directions for the model single-compartment cell at 31.4 Hz, for a vertical slice (*X* direction) of 3 mm centred along the rotating rod (See Fig. S3 for 62.8 Hz). All images have a field of view of (40 x 20) mm with a resolution of (128 x 64) pixels. The analysis is divided into two regions of interest (ROI). ROI_1 is considered as the space around the rotating rod, while ROI_2 comprises the space under the rod (see Fig. 1). In ROI_1 a flow pattern similar to that of a CC in a regime where Taylor vortices are formed is observed while in ROI_2 a large recirculation region can be identified. Velocities in the *Y* direction correspond to radial velocities while velocities along the *X* direction are assigned to azimuthal ones. Similar results were previously reported for different rotational speeds and cell dimensions [4].

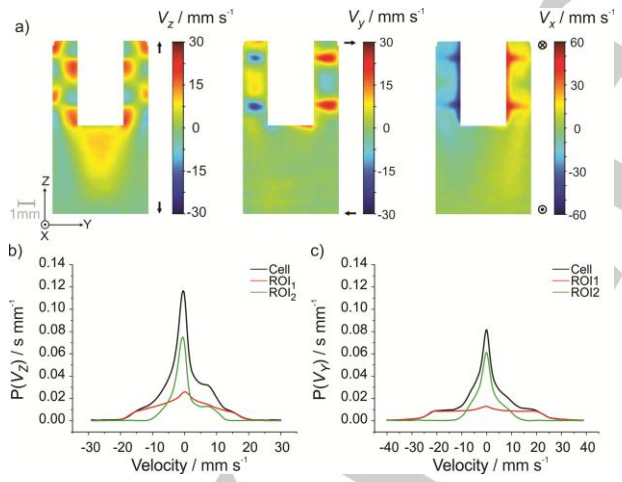

Figure 2: (color online) Velocity maps (a) and velocity propagators along *Z* (b) and *Y* (c) directions, acquired for the *Single compartment ECC* at a rotational speed of 31.4 Hz.

The main feature of ROI_1 is that the Taylor vortices appear interconnected in the *Z* direction. For such low rotation speed, this is not expected in a CC and is a consequence of the flow pattern of ROI_2. The fluid below the rotating rod moves upwards, while the recirculation towards the bottom of the cell is observed on the exterior. The up going liquid that reaches the lowest vortex resembles an injection of fluid in a CC. This behaviour has been described in detail by Vallatos et al. [18], where a Poiseuille flow is added by injecting liquid through the bottom of a CC. The main difference with this study is that in [18] the liquid leaves the cell through the top, while in our case it recirculates towards ROI_2. This flow pattern renders a very effective mixing mechanism which is essential for electrochemical measurements. Radial velocities (*Y*) present the characteristic jets flowing from the rotating rod towards the cell exterior in ROI_1, with a maximum velocity $v_Y = 25$ mm/s. For the azimuthal velocities, a maximum average velocity of $v_X = 55$ mm/s is detected near the rotating rod.

The velocity pattern can be further analyzed by the inspection of the probability distributions. The propagator for a displacement time $\Delta = 18$ ms in the *Z* direction (Fig. 2b) was acquired for the whole cell and for ROI_1 and ROI_2, by selecting different slices along the axial direction. In ROI_1 maximum velocities of 20 mm/s are observed, while the higher intensity at zero velocity along *Z* direction is due to the high amount of particles with purely azimuthal velocities. The obtained distribution is symmetric around zero amplitude velocities, in agreement with previous results [18]. The distribution in ROI_2 shows a maximum at a mean velocity $v_z = -0.94$ mm/s, as the volume occupied by the ones moving towards the bottom of the cell is larger than the one occupied by molecules moving upwards. The secondary maximum of $v_z = 7.5$ mm/s corresponds to the region below the rotating rod, as determined by a pixel by pixel examination of the velocity map. It should be noted that the propagator acquired for the whole cell matches the arithmetic addition of the propagators of ROI_1 and ROI_2.

Since the propagators in the X and Y directions give equivalent information due to the azimuthal symmetry of the cell, only $P(V_Y)$ is shown in Fig. 2c. In ROI_1, maximum velocities detected are of 40 mm/s in both directions, *Y* and *–Y*. Even though higher velocity amplitudes can be appreciated from the acquired velocity maps, the relative amount of particles associated to those velocity values is too small and their contribution to the flow propagator falls below the noise level. In ROI_2 the dominant velocity component is in *Z*, thus the propagator in *Y* presents a large intensity in zero velocity. The slight asymmetry in the flow pattern observed in the ROI_2 $P(V_Y)$ is responsible for the asymmetry of the cell propagator, as more regions present positive velocities rather than negative ones. This behaviour is heightened as rotation speed increases, as shown in the Supporting Information for a rotation of 62.8 Hz (Fig. S3b). In this direction the addition of the propagators also matches the data obtained from acquiring the whole sample, which is shown in the figure.

Biphasic ECC. Since the height of the biphasic ECC is longer than the sensitive volume defined by the MRI radiofrequency coil, only data concerning the lower part of the rotating rod and the liquid interface are shown. A full mapping of the flow on the whole cell can be obtained by displacing the cell in the MRI system for different experiments. This was measured as a preliminary test for a single phase flow and can be observed in Fig. S4 of the Supporting Information. The obtained velocity map shows that above the region delimited by the rf-coil sensitive volume, the hydrodynamics is dominated by the presence of counter-rotating vortices characteristic of a TVF regime, in agreement with previous results.[5] The shape and stability of the liquid|liquid interface was monitored using a reference image employing zero amplitude velocity gradients. Since 1,2-dichloroethane has a lower proton density than water, a

decrease in pixel intensity can be appreciated (See Fig. S5 of the Supporting Information). The inherent contrast between both phases was used to discriminate the velocity maps associated with each phase. In Fig. 3 we present the data separated along the *Z* direction, in order to show that the liquid|liquid interface remains flat during the NMR experiments, obtained for different rotation speeds.

Velocity maps in the *Z* direction are shown in Fig. 3. a-b for two rotation speeds. The velocity maps associated with the aqueous phase present a flow pattern similar to the one obtained for the Single Compartment ECC. At a rotation speed of 31.4 Hz an inflow from ROI_2 to ROI_1 is clearly observed (Fig. 3a), together with the presence of a recirculation region in ROI_2. Velocities of the up going stream of water have a maximum of $v_Z = 14$ mm/s approximately halfway between the bottom of the rotating rod and the interface, while in the vicinities of the rod $v_Z = 8$ mm/s. Clearly, at the rod's surface $v_Z = 0$.

The velocity map in the Z direction for a rotational speed of 62.8 Hz is presented in Fig. 3b (See Fig. S6 for X and Y directions). As can be observed, when the rotational velocity increases, the vortices in ROI_1 start to change their size and shape and the recirculation region shows a more notorious asymmetry along the axial direction. Velocities of the up going stream of water molecules is of $v_Z = 12$ mm/s near the bottom of the rotating rod (where the electrode would be placed in an operating ECC) and a maximum velocity of $v_Z = 26$ mm/s is observed.

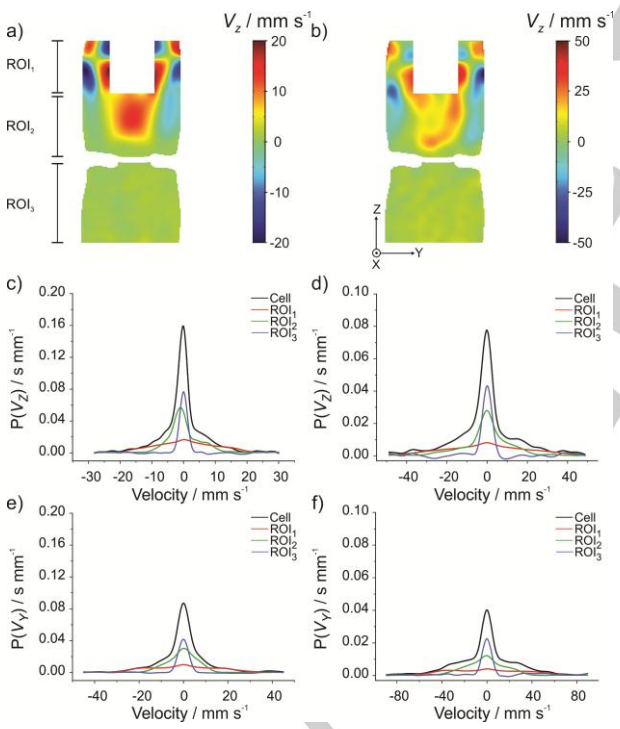

Figure 3. (color online) Velocity maps along de *Z* direction for 31.4 Hz (a) and 62.8 Hz (b) rotational speed and flow propagators along *Z* (c,d) and *Y* direction (e,f) for 31.4 Hz (c,e) and 62.8 Hz (d,f) rotational speed, acquired for the *Biphasic ECC*.

One particular feature of the obtained velocity maps is that for a low rotational speed the recirculation of fluid does not reach the liquid|liquid interface, as can be observed in Fig. 3a. As a greater convection flow is generated, the fluid in the proximity of the interface presents non-zero velocity. In particular, for a rotation speed of 62.8 Hz, near the liquid|liquid interface the velocity along the axial direction is about 4 mm/s (Fig. 3b).

Figure 3c and 3e show the propagators along *Z* and *Y* respectively, for a rotation speed of 31.4 Hz. The probability distribution in ROI_1 remains symmetric and resembles the one expected for Taylor vortices. Below the rotating rod (ROI_2) the distribution is shifted toward negative velocities in the Z direction, which corresponds to the fluid moving downwards through the outer regions of the cell while a significant population moving upwards with 8 mm/s is present. As a small fraction of the fluid has the maximum velocities, these are not detected, with the highest value of 20 mm/s present in $P(V_Z)$. For a higher rotation speed (62.8 Hz) (Fig. 3d and 3f) the propagators for the aqueous phase (ROI_1 and ROI_2) show that a high number of particles with larger velocities are present, where the main variation is observed for azimuthal velocities $P(V_Y)$.

When studying charge transfer process between the two phases, two possible mechanisms are stated: on one hand, a simple ion transfer reaction can take place, and on the other hand, the transfer may be facilitated by a neutral ligand present in the organic phase. In the case of simple ion transfer, the current is controlled by the diffusion of the ion in the aqueous phase, while in the facilitated ion transfer the current is controlled by the diffusion of the neutral ligand in the organic phase (See Supporting Information for further explanation on the ion transfer mechanisms). Consequently, the electrochemical response varies if the organic phase transport is only diffusive, that is, if the organic phase hydrodynamics is not affected by the movement of the aqueous phase. This information can be clearly seen from the obtained velocity maps in Fig. 3, where the organic phase is represented by ROI_3. It can be observed that in this region all data are within the noise level for both rotation speeds of the rod, thus assigned to zero velocity. Flow propagators on ROI_3 were acquired by the arithmetic subtraction of the cell propagator and the one associated with the aqueous phase (See Experimental Section).The obtained results are shown in Fig. 3, and exhibit a zero velocity distribution for both rotations speeds, supporting the assumption that a diffusive behavior of the organic phase is sustained in the lower compartment of the cell. The increase in the propagators width for a 62.8 Hz rotation speed is due to an increase in the field of flow employed in the experiments.

Biphasic ECC with four electrodes. We now turn our attention to the four-electrode ECC, with ITIES applications. Both electrochemical and NMR velocimetry experiments were performed in this cell. As schematized in Fig. 1c, two luggin capillaries are introduced, one in ROI_2 and the second one in ROI_3. Because of the cell asymmetry, both axial planes were imaged by NMR. Once again, the liquid|liquid interface could be determined by acquiring a reference image exhibiting an inherent contrast between the two fluids (Fig. S5b). As the height of the cell exceeds the NMR sensitive volume, the liquid|liquid interface was centered in the MRI coil and only this volume is analysed. Fig. 4 shows the velocity maps in *Z* for a rotation speed of 31.4 Hz and 62.8 Hz for two orthogonal imaging planes. (See Figs. S7-S8 for X and Y velocity maps). For a low rotation speed of the rod, the effect of the capillary is to screen the lower part of the cell. This behaviour can be clearly observed in the velocity maps along X and Y directions, where the fluid recirculation region is restricted to the area above the

luggin capillary. From Fig. 4a-b, it can be noticed that nearly zero amplitude velocities in the lower part of ROI_2 were detected. The effect of the capillary in the velocity distribution at 31.4 Hz rotational frequency is appreciated in more detail in the flow propagators presented in Fig. 5 a-b.

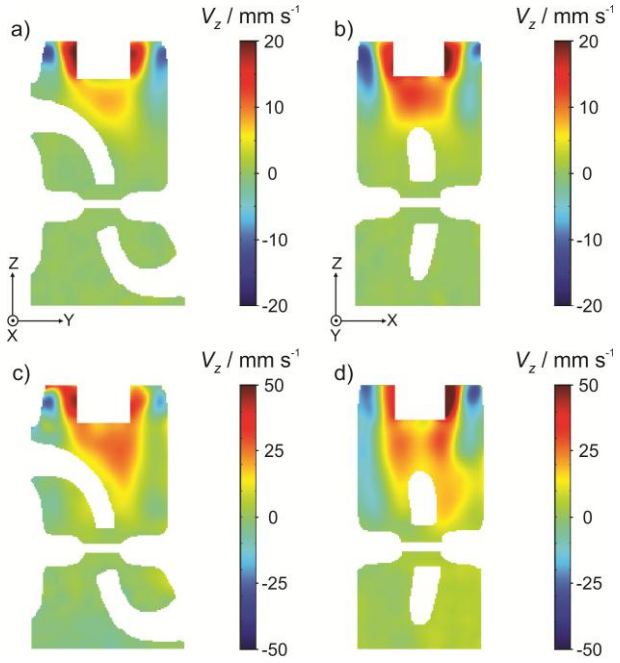

Figure 4. (color online) Velocity maps along the *Z* direction for 31.4 Hz (a, b) and 62.8 Hz (c,d) rotational speed, acquired for the *Biphasic ECC with four electrodes.* For each rotational velocity, a velocity map was acquired for the *Z-Y* (a,c) and the *Z-X* (c,d) plane.

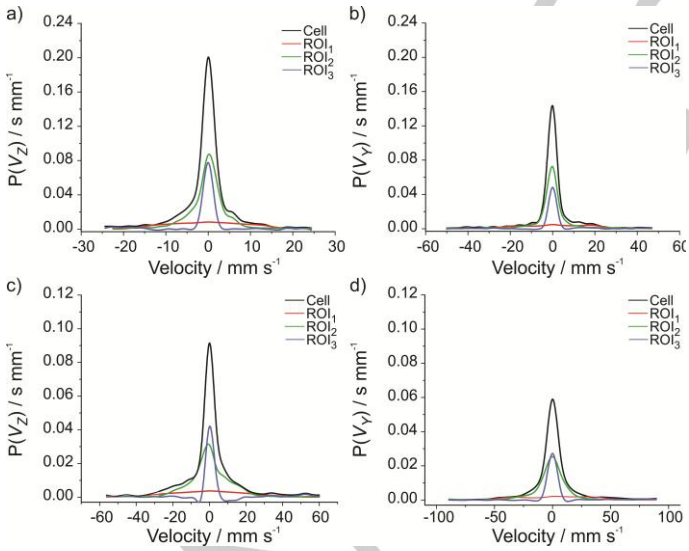

Figure 5. (color online) Flow propagators along the Z (a,c) and in Y direction (b,d) for 31.4 Hz (a,b) and 62.8 Hz (c,d) rotational speed, acquired for the *Biphasic ECC with four electrodes.*

A greater proportion of zero amplitude velocities can be observed in the ROI_2 propagators along the Z and Y directions. As the rotation speed increases, the flow induced by the rotating rod reaches the lower part of ROI_2. Even though the luggin capillary deviates the up-going stream of fluid, the velocity map along the axial direction exhibits a recirculating pattern similar to the one obtained for the biphasic ECC: the flow goes down along the vertical walls of the cell and recirculates towards the rotating rod (Fig.4 c-d). Flow propagators associated to the recirculating fluid (ROI_2) show a velocity distribution resembling the obtained results for the biphasic ECC.

The behaviour of the organic phase when forced hydrodynamic conditions are applied to the aqueous phase can be analyzed by the inspection of ROI_3 velocity maps (Fig. 4). The obtained flow patterns show negligible velocity amplitudes in the lower compartment of the cell, indicating that the organic phase is not affected by the agitation of the aqueous phase. Even though there is an apparent change, particularly for the right bottom of Fig. 4d, this corresponds to the noise level in these particular velocity maps. The increase in noise level is due to the change of the field of flow, which goes in detriment of the colour maps resolution. The quiescent state of the organic phase was further corroborated by the acquisition of flow propagators (Fig. 5), wherein the obtained results exhibit a zero velocity distribution, for both rotation speeds of the rod. The mechanical stability of the interface and the effect of convection on the organic phase can also be tested in terms of the electrochemical response. As previously stated, the two kinds of ion transfer reactions (simple or facilitated) have been widely used as model reactions, since they have been studied by many authors by means of different experimental and theoretical approaches [2f, 19]. In this work, these reactions will be employed to evaluate these physical effects.

Figure 6 shows cyclic voltammograms at the same forward sweep rate and different backward sweep rates for a simple ion transfer while the aqueous phase was stirred at 62.8 Hz. In this way, at the end of the forward scan, the amount of transferred ions is the same. A good agreement between experimental and simulated current-potential profiles -considering a reversible diffusion controlled mechanism for the ion transfer- is shown.
The analysis of the voltammograms obtained under these experimental conditions at different rotation speeds indicates that the backward peak current increases linearly with the

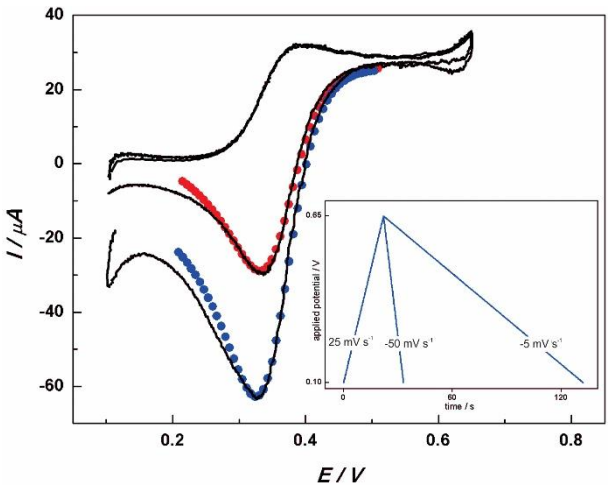

Figure 6. (color online) Cyclic voltammograms for the transfer of TEA^+ obtained under forced hydrodynamic conditions applied to aqueous phase (ω= 62.8 Hz). Forward scan: 0.025 V s^{-1} and backward scan: (●) 0.005 V s^{-1} and (●) 0.050 V s^{-1}. Solid circles correspond to a simulated current-potential profile considering only diffusional mass transport. Inset shows the different potential scans. Organic phase composition: 1.0×10^{-2} M TPAsDCC. Aqueous phase composition: KCl 1.0×10^{-2} M + 8.0×10^{-4} M TEABr

square root of the backward sweep rates (data are shown in Fig.S9 in the Supporting Information). This linear dependence is clear evidence that the mass transport in the organic phase only occurs by diffusion. It is also very important to remark that the slopes of the current peak plotted in Fig. S9, increase with the rotation speed. This is a consequence of the increase of ion accumulation on the organic side of the interface.

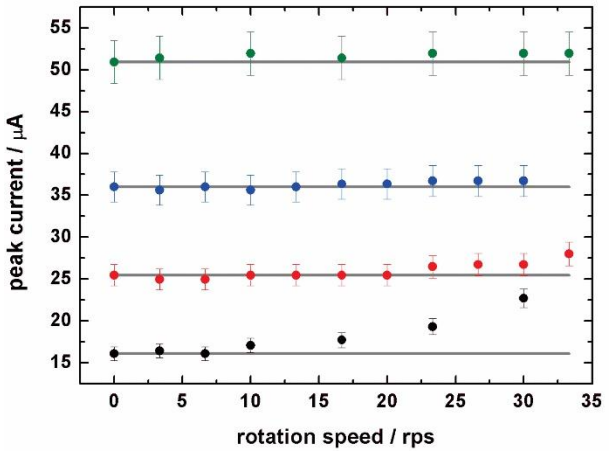

Figure 7. (color online) Peak current for the transfer of K^+ assisted by DB18C6 obtained under FHCs applied to aqueous phase at different sweep rates: (●) 0.010, (●) 0.025, (●) 0.050 and (●) 0.100 V s^{-1}. Solid lines correspond to the current peak obtained for quiescent solutions at different sweep rates. Organic phase composition: 1.0×10^{-2} M TPAsDCC + 2.0×10^{-3} M. Aqueous phase composition: KCl 1.0×10^{-2} M. Error bars are estimated by taking into account a 5% uncertainty for the peak current determination.

The most important differences between the stirred and unstirred experiments are observed at low sweep rates and when the current controlling species is present in the stirred phase [2f, 2i, 2j, 5]. It is important to remark that relatively low rotation speeds are enough to observe appreciable changes. In contrast, at high rotation speeds, the interface becomes unstable and oscillations in the current appear.

To show the extent of this mechanical effect, the facilitated transfer reaction can be employed. The peak current for this process was plotted as a function of rotation speed. Fig. 7 shows the peak current when forced hydrodynamic conditions are applied to the aqueous phase for the facilitated transfer of potassium ion by a ligand. When the aqueous phase is agitated and the current is controlled by the diffusion of the ligand in the organic phase, as long as a mechanical perturbation of the organic phase does not occur, the peak current coincides with that obtained under quiescent conditions. This behavior is observed for many different experimental conditions; however, a deviation of the expected value is seen for high rotation speeds (> 94.2 Hz). These conditions mark the limit for which the organic phase can be assumed to stay quiescent throughout the experiment for the glass cell used in this work.

Both electrochemical experiments, simple and facilitated ion transfer, are in full agreement with the results obtained by MRI. For the rotation speeds that have been imaged in this work, the organic phase, which is not stirred, does not present any measurable mechanical perturbation. In the case of electrochemical experiments, the interfacial signal is directly monitored, which is highly sensitive to mechanical instabilities, whereas MRI measurements allow the determination of the velocity fields throughout the cell. The correlation of these two independent measurements, electrochemical and velocimetry MRI, is a clear evidence of the high mechanical stability of the interface under forced hydrodynamic conditions. This stability ensures quiescent conditions to be maintained in the non-stirred phase. At this point the comparison between MRI and electrochemical measurements are qualitative. However simultaneous determinations of flow maps and electrochemical measurements inside the bore of a superconducting magnet can be readily carried out [20] and will be presented in future communications.

Conclusions

In this work, we report the first three-component velocity maps of a liquid|liquid system inside a four-electrode electrochemical cell. In order to fully characterize the hydrodynamics of this system, three different cell configurations were studied: *single compartment ECC*, *biphasic ECC* and finally, the *four-electrode ECC*. Velocimetry MRI and flow propagators were performed, demonstrating the ability of NMR experiments to obtain accurate information about the fluid dynamics inside an operating electrochemical cell. For the two biphasic cells configurations employed in this work, negligible velocities in the organic phase (1,2-dichloroethane) were found. The obtained results confirm that the organic phase hydrodynamics is not affected by the movement of the aqueous phase. This information was further corroborated with electrochemical experiments carried out using the same cell configuration and working at similar rotational frequency ranges.

Experimental Section

All experiments were performed on a 7.05 T Oxford superconducting magnet operating at a proton resonance frequency of 300.13 MHz. Excitation and detection were carried out with a 25 mm inner diameter Bruker GmbH birdcage coil with a length of 37 mm, using a 3D gradient coil system with a maximum gradient of 1.5 T/m from Bruker. For the 2D velocity maps measurements, a 3 mm slice in the x direction was excited, the field of view was set to 40 mm x 20 mm and matrices of size 128 x 64 were collected, resulting in an image resolution of (0.3125 mm x 0.3125 mm). For all imaging experiments, two signal acquisitions were collected and averaged. The most relevant parameters of the pulse sequence were the following: echo time: $t_E = 14$ ms, $\delta = 1$ ms and $\Delta = 2.2$ ms. For the acquired velocity maps typically the field of flow (FOF) was set to FOFx=100 mm/s, FOFy=40 mm/s, FOFz= 40mm/s for 31.4 rotational frequency and FOFx=220 mm/s, FOFy=120 mm/s, FOFz= 120mm/s for 62.8 Hz. Water doped with $CuSO_4$ was used in all experiments to reduce T_1 to approximately 100 ms. As the relaxation time of 1,2-dichloroethane is ~ 4.5 s for the characterization of biphasic systems, a recycle delay of 20 s was used to obtain signal from both, aqueous and organic phases. A static image of the system was used to create a mask from which the velocity maps were artificially separated. Because 1,2-dichloroethane has a lower proton density than water, a decrease in image intensity is observed in the lower compartment of the Biphasic cells (See Fig. S5 in the Supporting Information).

Flow propagator measurements were performed using the pulse sequence depicted in Fig. S2. Flow encoding gradients were applied with a duration (δ) and observation time (Δ) of 2.5 ms and 18 ms respectively. For all experiments *q-space* was sampled linearly in 32 steps and 8 signal acquisitions were averaged per experiment, with a recycle delay $T_R = 20\ s$. The flow propagator associated to the organic phase, given by

ROI_3, was obtained by the arithmetic subtraction between the propagator of the hole cell and the one related to the aqueous phase. To obtain only signal from the aqueous phase, a recycle delay of 500 ms was employed.

The electrochemical experiments were performed in a four-electrode system using a conventional glass cell of 0.25 cm^2 interfacial area. Two platinum wires were used as counter-electrodes; the reference electrodes were Ag|AgCl|Cl^-. The reference electrode in contact with the organic solution was immersed in an aqueous solution of 1.0 x 10^{-2} M tetraphenylarsonium chloride (TPAsCl) (Merck p.a.). The potential values reported (*E*) are the potentials applied including the transfer of the reference ion TPA^+. The supporting electrolytes are KCl (J.T. Baker p.a.), in ultrapure water, and tetraphenylarsonium dicarbollylcobaltate (TPAsDCC) in 1,2-dichloroethane, 1,2-DCE, (Dorwil p.a.). TPAsDCC was prepared as described in ref. [21]. Tetraethylammonium bromide (TEABr) -Mallinckrodt-, and dibenzo-18-crown-6 (DB18C6) -Sigma- were commercially available and used without further purification.

Cyclic voltammetry was carried out using a potentiostat which automatically eliminated the *iR* drop by means of a periodic current-interruption technique[22]. Forced hydrodynamic conditions (FHCs) were applied with a polytetrafluoroethylene (PTFE) cylinder (analogue to a rotating-disc electrode) controlled by a PINE disc rotator[2f].

Acknowledgements

We thank the financial support from CONICET, SeCyT Universidad Nacional de Córdoba, ANPCYT PICT 2010-096/2274 and PICT 2012-1820. M.R. Serial and F.M. Zanotto thank CONICET for their fellowships.

Keywords: Electrochemical cells • velocimetry MRI • Flow propagators • forced hydrodynamic conditions • ion transfer

[1] aJ. Koryta, *Electrochimica Acta* **1979**, *24*, 293-300; bZ. Samec, *Pure and applied chemistry* **2004**, *76*, 2147-2180; cR. A. Iglesias, S. A. Dassie, *Ion transfer at liquid/liquid interfaces*, Nova Science Publ., **2010**; dP. Peljo, H. H. Girault, *Encyclopedia of Analytical Chemistry*.

[2] aJ. A. Manzanares, R. Lahtinen, B. Quinn, K. Kontturi, D. J. Schiffrin, *Electrochimica acta* **1998**, *44*, 59-71; bB. Kralj, R. A. Dryfe, *The Journal of Physical Chemistry B* **2002**, *106*, 6732-6739; cK. Fujii, S. Tanibuchi, S. Kihara, *Analytical sciences* **2005**, *21*, 1415-1420; dB. Kralj, R. A. Dryfe, *Journal of Electroanalytical Chemistry* **2003**, *560*, 127-133; eM. j. Velický, K. Y. Tam, R. A. Dryfe, *Analytical chemistry* **2012**, *84*, 2541-2547; fN. Wilke, R. A. Iglesias, S. G. Chesniuk, S. A. Dassie, A. M. Baruzzi, *Bulletin of the Chemical Society of Japan* **2002**, *75*, 235-240; gM. A. Fernández, L. M. Yudi, A. M. Baruzzi, *Electroanalysis* **2004**, *16*, 491-496; hR. Fernández, S. Dassie, *Journal of Electroanalytical Chemistry* **2008**, *624*, 121-128; iR. Fernández, M. Velasco, L. Rossi, S. Dassie, *Journal of Electroanalytical Chemistry* **2010**, *650*, 47-54; jJ. M. Ovejero, R. A. Fernández, S. A. Dassie, *Journal of Electroanalytical Chemistry* **2012**, *666*, 42-51; kF. V. Mercado, J. M. Ovejero, R. A. Fernández, S. A. Dassie, *Journal of Electroanalytical Chemistry* **2016**, *765*, 100-104.

[3] aP. Mandin, T. Pauporté, P. Fanouillère, D. Lincot, *Journal of Electroanalytical Chemistry* **2004**, *565*, 159-173; bA. Alexiadis, A. Cornell, M. Dudukovic, *Journal of Electroanalytical Chemistry* **2012**, *669*, 55-66; cJ. Gonzalez, C. Real, L. Hoyos, R. Miranda, F. Cervantes, *Journal of electroanalytical chemistry* **2011**, *651*, 150-159; dC. A. Real-Ramirez, R. Miranda-Tello, L. F. Hoyos-Reyes, J. I. Gonzalez-Trejo, *International Journal of Chemical Reactor Engineering* **2010**, *8*.

[4] M. Carpinella, M. I. Velasco, E. V. Silletta, J. M. Ovejero, S. A. Dassie, R. H. Acosta, *Journal of Electroanalytical Chemistry* **2015**, *750*, 100-106.

[5] F. V. Mercado, J. Ovejero, F. Zanotto, M. Serial, M. Velasco, R. Fernández, R. Acosta, S. Dassie, *Journal of Electroanalytical Chemistry* **2017**, *791*, 64-74.

[6] aV. Lim, A. M. Hobby, M. J. McCarthy, K. L. McCarthy, *Chemical Engineering Science* **2015**, *137*, 1024-1033; bM. M. Britton, in *Nuclear Magnetic Resonance*, **2016**, pp. 164-189; cS. Stapf, S.-I. Han, *NMR imaging in chemical engineering*, John Wiley & Sons, **2006**; dJ. Perlo, E. V. Silletta, E. Danieli, G. Cattaneo, R. H. Acosta, B. Blümich, F. Casanova, *Magnetic resonance imaging* **2015**, *33*, 328-335; eC. Binter, U. Gülan, M. Holzner, S. Kozerke, *Magnetic resonance in medicine* **2016**, *76*, 191-196; fM. M. Britton, *Progress in Nuclear Magnetic Resonance Spectroscopy* **2017**.

[7] M. Nemri, S. Charton, E. Climent, *Chemical Engineering Science* **2016**, *139*, 109-124.

[8] S. G. Huisman, D. P. van Gils, C. Sun, *European Journal of Mechanics-B/Fluids* **2012**, *36*, 115-119.

[9] G. I. Taylor, *Philosophical Transactions of the Royal Society of London. Series A, Containing Papers of a Mathematical or Physical Character* **1923**, *223*, 289-343.

[10] M. Lopez-Gonzalez, W. Holmes, P. Callaghan, *Soft Matter* **2006**, *2*, 855-869.

[11] J. Novak, M. M. Britton, *Soft Matter* **2013**, *9*, 2730-2737.

[12] J. D. Seymour, B. Manz, P. T. Callaghan, *Physics of Fluids* **1999**, *11*, 1104-1113.

[13] A. L. Broadbent, J. M. Mullin, S. L. Codd, J. D. Dockery, J. D. Seymour, *Applied Magnetic Resonance* **2012**, *42*, 137-152.

[14] P. Callaghan, C. Eccles, Y. Xia, *Journal of Physics E: Scientific Instruments* **1988**, *21*, 820.

[15] V. Mareček, Z. Samec, J. Koryta, *Advances in colloid and interface science* **1988**, *29*, 1-78.

[16] P. T. Callaghan, *Translational dynamics and magnetic resonance: principles of pulsed gradient spin echo NMR*, Oxford University Press, **2011**.

[17] P. R. Moran, *Magnetic resonance imaging* **1982**, *1*, 197-203.

[18] A. Vallatos, M. C. Wilson, A. F. Taylor, M. M. Britton, *EPL (Europhysics Letters)* **2012**, *99*, 68001.

[19] aT. Wandlowski, V. Mareček, Z. Samec, *Electrochimica Acta* **1990**, *35*, 1173-1175; bS. Kihara, M. Suzuki, K. Maeda, K. Ogura, S. Umetani, M. Matsui, Z. Yoshida, *Analytical Chemistry* **1986**, *58*, 2954-2961; cA. Berduque, A. Sherburn, M. Ghita, R. A. Dryfe, D. W. Arrigan, *Analytical chemistry* **2005**, *77*, 7310-7318; dG. Bouchard, P. A. Carrupt, B. Testa, V. Gobry, H. H. Girault, *Pharmaceutical research* **2001**, *18*, 702-708; eA Juárez, A. Baruzzi, L. Yudi, *Journal of Electroanalytical Chemistry* **2005** *577*, 281-286; fQ. Li, S. Xie, Z. Liang, X. Meng, S. Liu, H. H. Girault, Y. Shao, *Angewandte Chemie International Edition* **2009**, *48*, 8010-8013; gM. Rimboud, K. Charreteur, V. Sladkov, C. Elleouet, F. Quentel, M. L'Her, *Journal of Electroanalytical Chemistry* **2009**, *636*, 53-59; hY. Wang, J. Velmurugan, M. V. Mirkin, P. J. Rodgers, J. Kim, S. Amemiya, *Analytical chemistry* **2009**, *82*, 77-83; iL. Sinru, H. Freiser, *Journal of electroanalytical chemistry and interfacial electrochemistry* **1985**, *191*, 437-439; jY. Shao, M. Osborne, H. Girault, *Journal of electroanalytical chemistry and interfacial electrochemistry* **1991**, *318*, 101-109; kQ.-Z. Chen, K. Iwamoto, M. Senō, *Electrochimica acta* **1992**, *37*, 643-646; lM. D. Osborne, H. H. Girault, *Electroanalysis* **1995**, *7*, 425-434; mP. Beattie, A. Delay, H. Girault, *Electrochimica acta* **1995**, *40*, 2961-2969; nP. Beattie, R. Wellington, H. Girault, *Journal of Electroanalytical Chemistry* **1995**, *396*, 317-323; oY. Shao, M. V. Mirkin, *Journal of the American Chemical Society* **1997**, *119*, 8103-8104; pR. Iglesias, S. A. Dassie, L. M. Yudi, A. M. BARUZZI, *Analytical sciences* **1998**, *14*, 231-236; qY. Yuan, Z. Gao, J. Guo, Y. Shao, *Journal of Electroanalytical Chemistry* **2002**, *526*, 85-91; rM. J. Stephenson, A. J. King, S. M. Holmes, R. A. Dryfe, *The Journal of Physical Chemistry B* **2005**, *109*, 19377-19384.

[20] aJ. M. Bray, A. J. Davenport, K. S. Ryder, M. M. Britton, *Angewandte Chemie International Edition* **2016**, *55*, 9394-9397; bA. J. Ilott, N. M. Trease, C. P. Grey, A. Jerschow, *Nature communications* **2014**, *5*, 4536

[21] A. M. Baruzzi, H. Wendt, *Journal of Electroanalytical Chemistry and Interfacial Electrochemistry* **1990**, *279*, 19-30.

[22] A. Baruzzi, J. Ühlken, *Journal of Electroanalytical Chemistry and Interfacial Electrochemistry* **1991**, *282*, 267-273.